Available online at www.CivileJournal.org

Civil Engineering Journal

(E-ISSN: 2476-3055; ISSN: 2676-6957)

Vol. 10, No. 05, May, 2024

Effect of Steel Fiber on Plastic Hinge Length of Concrete Columns: Buckingham Theory Application

Tavio [1], Bambang Sabariman [2*], Slamet Widodo [3]

[1] *Department of Civil Engineering, Institut Teknologi Sepuluh Nopember, Surabaya, 60111, Indonesia.*

[2] *Department of Civil Engineering, Universitas Negeri Surabaya, 60231, Indonesia.*

[3] *Department of Civil Engineering, Universitas Negeri Yogyakarta, 55281, Indonesia.*

Received 19 January 2024; Revised 18 April 2024; Accepted 24 April 2024; Published 01 May 2024

Abstract

The accuracy of designing the performance of concrete structures nowadays not only depends on the use of standard materials (cement, sand, and gravel) for certain concrete strengths but also on the accuracy of using additional materials for concrete, such as steel fiber. The use of steel fiber not only can improve the performance of concrete structures to behave in a ductile manner but can also form plastic hinges according to design purposes. The design of the axial load of $P_a=0.121.A_g.f'_c$ is based on the prediction of the column's axial capacity. The columns were designed to behave in a flexural manner. As predicted, the lengths of the plastic hinges were found not too long. Controlling the length of plastic hinges in the design of structural concrete members is necessary to avoid excessive displacements. The control is mainly related to the prediction of the plastic hinge length. Thus, in this case, a plastic hinge length formula is required. In the study, the length of the plastic hinges of columns, which are confined with square stirrups and reinforced with steel fiber with V_f = 0%, 0.5%, 1%, 1.5%, and 2%, is proposed. This plastic hinge length formula is proposed after all column test specimens have met the displacement ductility requirement of $m_D>4$, meaning that all test specimens are defined as very ductile.

Keywords: Buckingham Theory; Disaster Risk Reduction; Ductility; Performance; Plastic Hinge Length; Steel Fiber.

1. Introduction

Earthquakes are natural events that cannot be stopped on this earth. Therefore, they will continue to occur repeatedly. Ironically, the impact of this earthquake is extraordinary, both on infrastructure and property and even causing loss of life. The largest earthquake in this century occurred in Turkey, precisely on Monday, February 6th, 2023. An earthquake measuring 7.8 on the Richter scale occurred, killing more than 3,823 people; 14,500 people were injured; and 4,900 buildings were razed to the ground [1]. This large number of collapsed buildings could be due to the fact that the fact that many of the buildings built were not earthquake-resistant. Some buildings collapsed due to earthquakes were due to they were not designed properly to withstand the severe earthquakes [2], especially in column-beam connections, column damage, failure to fulfill the column-to-beam strength ratio in the beam-column joint (BCJ), namely 6/5 or 1.20 [3], and the formation of plastic hinges. Retrofitting purposes can be taken to solve these existing incompliances [4, 5]. However, preventive measures starting with the selection of materials, methods, and design stage are still more preferable.

Plastic hinges are areas defined at a distance equal to twice the depth of the component from the face of the column or beam and also include other sections in walls, frames, and slabs where yielding of reinforcement can occur as a result

* Corresponding author: bambangsabariman@unesa.ac.id

http://dx.doi.org/10.28991/CEJ-2024-010-05-03

of lateral displacement. When an earthquake occurs in certain circumstances where the earthquake shock has greatly influenced the deformation of the structure, these plastic hinges must form so much before the building collapses. The first plastic hinges must be formed in the beam elements first, then in the columns on the bottom floor of the building. The formation of plastic hinges is governed by several factors influencing the length of the plastic hinge [6], such as (a) axial load level; (b) moment gradient; (c) shear stress in the plastic hinge region; (d) amount and mechanical properties of longitudinal and transverse reinforcement; (e) strength of concrete; and (f) confinement level provided in the potential plastic hinge zone.

Indirectly, this factor causes bending and shear forces, which affect the shape and length of the plastic hinge. Meanwhile, predicting the length of a plastic hinge is difficult because it depends on the characteristic parameters of the concrete and reinforcement. This plastic hinge is an interesting topic for engineers because of plastic deformation [7]. The deformation causes rotation due to shear forces or bending moments. The formation of the rotation of the plastic hinge is also caused by the influence of longitudinal reinforcement [8]. The results from other researchers show that the axial load ratio, shear span depth ratio, and longitudinal reinforcement ratio greatly influence the lateral load-displacement response and the length of the plastic hinge [9, 10].

Apart from that, the moment gradient factor, the influence of tensile shear and strain penetration, the mechanical attributes of transverse reinforcement, the strength of concrete and steel, the level of concrete confinement, and what cannot be avoided are the complex nonlinear properties of materials. Therefore, determining the correct length of the plastic hinge (l_p) encounters several obstacles [11]. The complex nature of the material is an obstacle in determining the length of the plastic hinge, even though currently steel fiber is increasingly being used as an additional material in concrete. Thus, it is logical (like it or not) that steel fiber is also a parameter in determining the length of a plastic hinge. Research on the effect of steel fiber with a fiber volumetric ratio (V_f) = 1-2% has been attempted [12]. However, it has not yet produced a formula for the length of the plastic hinge.

Several parameters, including A_g, A_s, D, h, d_b, f '$_c$, f_y, L, P, and P_o, are still used as determinants of the plastic hinge length formula [13–27], where A_g = gross area, A_s = area of reinforcement, D = cross-sectional diameter of column, h = cross-sectional height of beam or column, d_b = longitudinal reinforcement diameter, f'$_c$ = compressive strength of concrete, f_y = yield stress of steel reinforcing bars, L = column length between point of contraflexure and the point of maximum moment, P = column axial force, P_o=0.85.f 'c.(A_g–A_s)+f_y. A_s = nominal axial force. Based on this fact, it can be seen that almost all plastic hinge length formulas do not accommodate the use of steel fiber in their formulation. Hence, it can be said that there is still a gap in the use of concrete materials with the length of plastic hinges. For this reason, this research was carried out to fill this gap. In this case, the strength of concrete nowadays is not only influenced by standard concrete materials, such as cement, sand, and gravel, but also depends on the accuracy of the design according to the performance requirements of the concrete structures, such as the inclusion of additional materials in the concrete.

Foundations, columns, beams, walls, and roofs can still fail as a result of being struck by an earthquake. However, the failure of a structural column will cause the failure of a structure as a whole. Therefore, the structural column must be designed to be earthquake-resistant. The earthquake forces on the column cause the column to experience excessive displacement, and plastic hinges occur around the column joints. The area around the column joint is critical and must be designed carefully so that it can absorb earthquake energy [28]. The inability to absorb earthquake energy will cause serious damage to the column structure. When a building experiences an earthquake, the shear force that occurs will be borne as a whole by the column; this will continue until plastic hinges occur in the column. It should be noted that for a building to be categorized [29] as an earthquake-resistant building, the building must be able to dissipate energy due to earthquakes.

One way for a building to remain sturdy when a large earthquake occurs is through the formation of many plastic hinges [13] before the building collapses. This is one of the philosophies of designing earthquake-resistant buildings where the building is allowed to experience damage through the formation of plastic hinges which are quite widely distributed in all building elements, but are expected not to collapse so that the building is ductile [30-33] at the required earthquake load limits. The ductility of this building can be achieved if the building is designed to resist forces well, including The building is designed according to SDC (seismic design category), adequate ratio of main reinforcement of beams and columns, and adequacy of confinement [34]. The adequacy of confinement can affect ductility [35, 36], both curvature ductility (μ_φ) and displacement ductility (μ_Δ). Several researchers made criteria for ductility displacement as follows [37]: high ductile: μ_Δ>4, moderate ductile: 2≤μ_Δ≤4, low ductile: 2<μ_Δ. However, a building can be categorized as earthquake-resistant if the building can dissipate earthquake energy through the formation of many plastic hinges before the building collapses. Observing the plastic hinges of the column also observes the location and length of the plastic hinges. The length of the plastic hinge (l_p) must be controlled to avoid excessive displacement.

The results of the curvature measurement of structural members can be used to determine the length of the plastic hinges of structural members [38]. This means that there is a relationship between the curvature and the length of the plastic hinges. For this reason, in this research, a set of measurement methods that use a curvature measuring device together with a recorder unit has been designed.

2. Material and Methods

2.1. Specimen

The column test specimens were defined by several variations, including 1). Columns are differentiated by the spacing of the confining stirrups at (s_h)=50 mm, 65 mm, and 80 mm, 2). Concrete in columns is also differentiated between reinforced concrete columns without steel fiber (SF) and those using SF, 3). The use of SF is based on V_f, namely V_f = 0, 0.5, 1, 1.5, and 2% (see Table 1). The column reinforcement in Figure 1 has been adapted to American Concrete Institute (ACI) 318-19, including all reinforcement used using threaded reinforcement, the first confining stirrup from the face of the column was placed at a maximum spacing of 50 mm. In the study, the confining stirrups were installed at 35 mm, and the test area was adjusted to the length of the plastic hinge, which is equal to 2h = 2×200 = 400 mm, h is the dimension of the column, the anchorage length is made at 40D_{ef}, D_{ef} is the effective diameter of steel reinforcement, while the column longitudinal reinforcement ratio (ρ_s) is 2.48%. All hook shapes are made at 1350 and the column anchorage direction is adjusted to the direction of the quasi-cyclic load [39]. The horizontal load (P_h) which is considered to represent earthquake lateral forces or quasi-cyclic forces is placed at a height of 800 mm based on the flexural failure design with a value of flexural-to-shear strength ratio FSSR<0.6, namely $FSSR_1$=0.31, $FSSR_2$=0.376, and $FSSR_3$=0.433. The $FSSR_1$ value corresponds to a confinement spacing of s_h = 50 mm, $FSSR_2$ corresponds to a confinement spacing of s_h = 65 mm, and $FSSR_3$ corresponds to a confinement spacing of s_h = 80 mm (Table 2).

This research included three and twelve column test specimens without SF and with SF, respectively. Based on the stirrup distance s_h = 50-80 mm, a confinement value (Z_m) = 20.24-40.26 were obtained. Thus, the column behaved in a flexural manner. The FSSR value is taken<0.6. All column specimens were then tested with quasi-cyclic loads until the column failed. Hence, based on these data, fifteen column test specimens were designed as detailed in Table 1, and Figures 1 and 2. Tensile tests of reinforcing steels are shown in Figure 3. The flowchart of the research procedure is given in Figure 4.

Table 1. Details of specimens

No.	Specimen ID	b=h (mm)	L (mm)	Main reinforcement	Stirrups		V_f steel fiber	f_y (MPa)	f_{yh} (MPa)	$f'_{c\text{-average}}$ (MPa)	$A_{sh\text{-}1\text{-}ACI}$ (mm^2)	$A_{sh\text{-}2\text{-}ACI}$ (mm^2)	$A_{sh\text{-}provided}$ (mm^2)
					d_s (mm)	s_h (mm)							
1	Col.1.a	200	800	8D13	8	50	0	405.87	546.83	27	46.17	36.06	93.33
2	Col.1.b	200	800	8D13	8	50	0.5%	317.01	344.30	27	73.45	57.37	86.67
3	Col.1.c	200	800	8D13	8	50	1%	405.87	546.83	27	46.17	36.06	93.33
4	Col.1.d	200	800	8D13	8	50	1.5%	317.01	344.30	27	73.45	57.37	86.67
5	Col.1.e	200	800	8D13	8	50	2%	405.87	546.83	27	46.17	36.06	93.33
6	Col.2.a	200	800	8D13	8	65	0	405.87	546.83	27	60.02	46.88	93.33
7	Col.2.b	200	800	8D13	8	65	0.5%	317.01	344.30	27	95.48	74.58	86.67
8	Col.2.c	200	800	8D13	8	65	1%	405.87	546.83	27	60.02	46.88	93.33
9	Col.2.d	200	800	8D13	8	65	1.5%	317.01	344.30	27	95.48	74.58	86.67
10	Col.2.e	200	800	8D13	8	65	2%	405.87	546.83	27	60.02	46.88	93.33
11	Col.3.a	200	800	8D13	8	80	0	405.87	546.83	27	73.87	57.69	93.33
12	Col.3.b	200	800	8D13	8	80	0.5%	317.01	344.30	27	117.52	91.79	86.67
13	Col.3.c	200	800	8D13	8	80	1%	405.87	546.83	27	73.87	57.69	93.33
14	Col.3.d	200	800	8D13	8	80	1.5%	317.01	344.30	27	117.52	91.79	86.67
15	Col.3.e	200	800	8D13	8	80	2%	405.87	546.83	27	73.87	57.69	93.33

Note Col.1= s_h 50 mm, Col.2= s_h 65 mm, Col.3= s_h 80 mm, a=V_f 0%, b=V_f 0.5%, c=V_f 1%, d=V_f 1.5%, e=V_f 2%, b=h= cross section of column, d_s=diameter of stirrups, A_{sh}=area of stirrups, f_{yh} = yield strength of stirrups.

Table 2. Classification of failure mechanisms [40]

	Transverse reinforcement details		
	ACI conforming details with 135° hooks	Closed hoops with 90° hooks	Other (including lap-spliced transverse reinforcement)
FSSR ≤ 0.6	Flexure	Flexure-shear	Flexure-shear
0.6 < FSSR ≤ 1.0	Flexure-shear	Flexure-shear	Shear
FSSR > 1.0	Shear	Shear	Shear

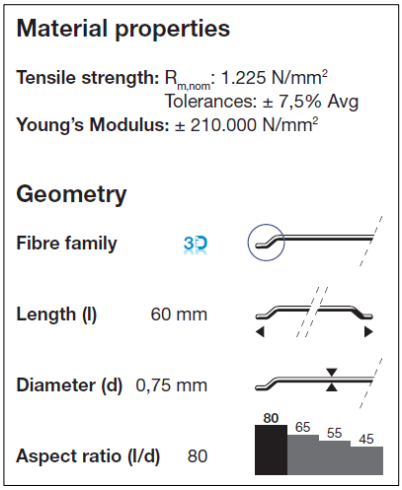

(a) Steel fiber used was a manufacturer's product

(b) Reinforcement of column specimen

Figure 1. Photograph of steel fiber with aspect ratio l/d = 80 and specimen reinforcement of column

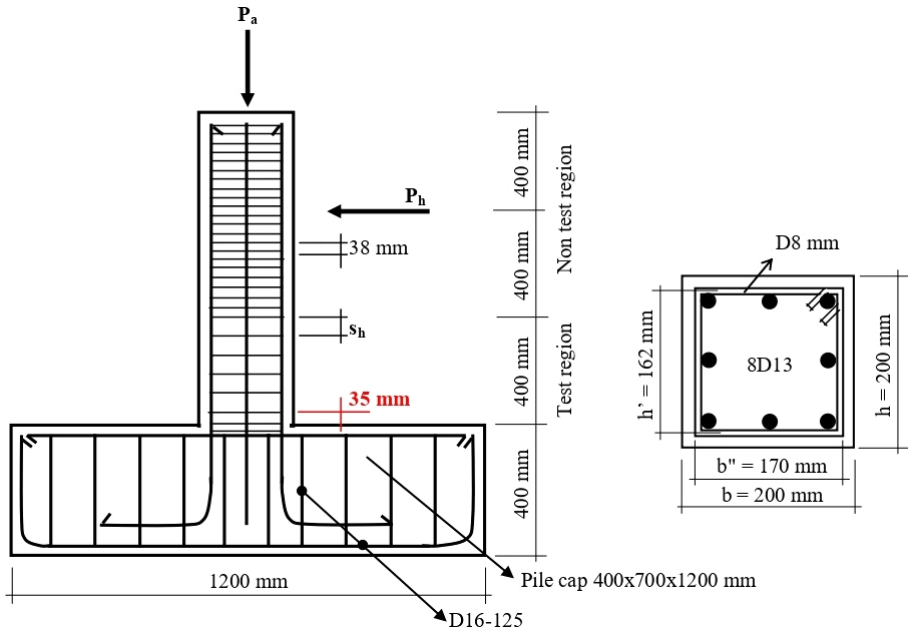

Figure 2. Details of specimen reinforcement

Figure 3. Tensile tests of reinforcing steels

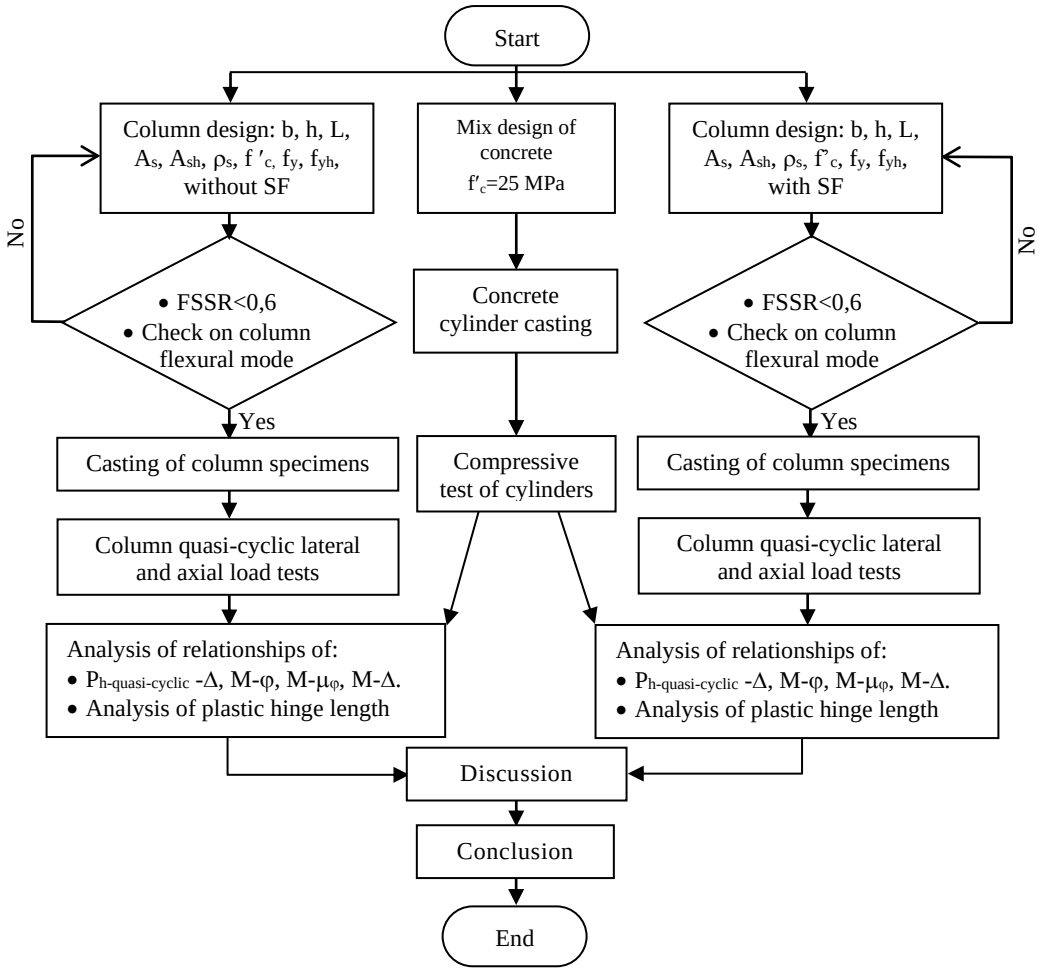

Figure 4. Flowchart of research procedure

2.2. Tensile Test Results of Reinforcing Steels

The tensile steel test is applied to all types of column reinforcing steel, namely D8, D13, and D16 reinforcement. The gage length is 200 mm according to the Indonesian National Standard (SNI) 2052:2017 [41]. A Micro Computer Universal Testing Machines (MC-UTM) with a capacity of 200 tons was used for tensile tests. The tensile test results are shown in Tables 3 to 6. These results indicate that the reinforcing steel bars for stirrups have satisfied the requirements of the Indonesian National Standard [41] in this case, including the elongation value of D8 and D13 reinforcement > 11%, while the yield strength of the stirrups (f_{yh}) of D8 reinforcement is < 700 MPa and the yield strength (f_y) of D13 reinforcement is < 420 MPa. Thus, all of the steel bars are suitable for use as reinforcement of the test specimens. Specifically, for the tensile test of D16 reinforcing steel, the results are not displayed even though the data is available.

Table 3. Specifications of D8 steel bars for transverse reinforcement (stirrups) of specimens # 4-6, 10-12

No.	Sample ID	D_{ef} (mm)	f_{yh} (MPa)	$f_{y\text{-}max}$ (MPa)	Ratio ($f_{y\text{-}max}/f_{yh}$)	Elongation (%)
1	St.81-1	7.43	324.01	431.72	1.33	22.00
2	St.81-2	7.44	319.92	421.35	1.32	19.00
3	St.81-3	7.42	307.09	406.71	1.32	20.00
	Average	7.43	317.01	419.93	1.32	20.33

Table 4. Specifications of D8 steel bars for transverse reinforcement (stirrups) of specimens # 1-3, 7-9, 13-15

No.	Sample ID	D_{ef} (mm)	f_{yh} (MPa)	$f_{y\text{-}max}$ (MPa)	Ratio ($f_{y\text{-}max}/f_{yh}$)	Elongation (%)
1	St.82-1	7.75	543.57	673.80	1.24	24.42
2	St.82-2	7.76	525.88	657.82	1.25	27.93
3	St.82-3	7.61	571.04	711.84	1.25	22.29
	Average	7.71	546.83	681.15	1.25	24.88

Table 5. Specifications of D13 steel bars for longitudinal reinforcement of specimens # 4-6, 10-12

No.	Sample ID	D_{ef} (mm)	f_y (MPa)	$f_{y\text{-}max}$ (MPa)	Ratio ($f_{y\text{-}max}/f_y$)	Elongation (%)
1	St.13.1-1	12.69	340.56	471.26	1.38	27.00
2	St.13.1-2	12.70	344.06	465.75	1.35	25.00
3	St.13.1-3	12.71	348.29	469.47	1.35	25.00
	Average	12.70	344.30	468.83	1.36	25.67

Table 6. Specifications of D13 steel bars for longitudinal reinforcement of specimens # 1-3, 7-9, 13-15

No.	Sample ID	D_{ef} (mm)	f_y (MPa)	$f_{y\text{-}max}$ (MPa)	Ratio ($f_{y\text{-}max}/f_y$)	Elongation (%)
1	St.13.2-1	12,48	418,87	659,28	1,57	23,82
2	St.13.2-2	12,64	381,64	603,52	1,58	36,68
3	St.13.2-3	12,64	417,12	670,93	1,61	20,54
	Average	12,58	405,87	644,57	1,59	27,01

2.3. Mix Design and Concrete Compression Test Results

The design compressive strength of the concrete is 25 MPa, to maintain uniformity in achieving concrete strength. In this study, ready-mix concrete products were used, the mix design is shown in Table 7. The size of the concrete cylinder used is 150 mm in diameter with a height of 300 mm. Six cylinders were tested with the mix design shown in Table 7. After casting the column and cylinder test specimens for 28 days, the compressive tests were carried out (Table 8 and Figure 5).

Table 7. Mix design of concrete f_c' 25 MPa for 1 m^3 volume

No.	Materials	1 m^3 SSD (kg/m^3)
1	Cement, OPC type 1	322
2	Fly ash, ex. Jepara (Indonesia)	57
3	Sand, ex. Merapi (Indonesia)	823
4	Coarse Agg., ex. Merapi (Indonesia) split size 10-20 mm	962
5	Water	170
6	Admixture, Sika VZ (Indonesia)	1.22
	Density	**2335**

Note: SSD = saturated surface dry, concrete used was a manufacturer's product

Table 8. Compressive strength of concrete

No.	Specimen	Compressive strength of concrete (MPa)
1	S_1	26.07
2	S_2	29.95
3	S_3	24.96
4	S_4	26.45
5	S_5	27.8
6	S_6	26.77
	Average	27.00

Figure 5. Concrete compression test setup

Based on the diameter values of stirrup reinforcement, longitudinal reinforcement, V_f, f_y, f_{yh}, s_h, f'_c, and column cross-section. The Z_m value can be then calculated [42], and the peak stress of steel-fiber reinforced concrete (f'_{ccf}) value due to the use of steel fiber is also computed [43], while for effect of confining steel can also be obtained [44-46]. The results from the calculations are given in Table 9.

Table 9. f'_{ccf} value due to the use of steel fiber

No.	Specimen ID	s_h (mm)	f_y (MPa)	f_{yh} (MPa)	f'_c (MPa)	Z_m	V_f	f'_{ccf} (MPa)
1	Col.1.a	50	405	546	27	20.51	0	32.21
2	Col.1.b	50	317	344	27	20.24	0.5%	30.67
3	Col.1.c	50	405	546	27	20.51	1%	32.18
4	Col.1.d	50	317	344	27	20.24	1.5%	29.81
5	Col.1.e	50	405	546	27	20.51	2%	39.01
6	Col.2.a	65	405	546	27	29.98	0	30.01
7	Col.2.b	65	317	344	27	29.53	0.5%	28.89
8	Col.2.c	65	405	546	27	29.98	1%	29.55
9	Col.2.d	65	317	344	27	29.53	1.5%	28.08
10	Col.2.e	65	405	546	27	29.98	2%	35.82
11	Col.3.a	80	405	546	27	40.26	0	28.76
12	Col.3.b	80	317	344	27	39.60	0.5%	28.16
13	Col.3.c	80	405	546	27	40.26	1%	28.47
14	Col.3.d	80	317	344	27	39.60	1.5%	27.36
15	Col.3.e	80	405	546	27	40.26	2%	34.50

Note Col.1= s_h 50 mm, Col.2= s_h 65 mm, Col.3= s_h 80 mm, a=V_f 0%, b=V_f 0.5%, c=V_f 1%, d=V_f 1.5%, e=V_f 2%.

2.4. Curvature Measuring Procedure

As a result of the quasi-cyclic loading (actuator) on all test specimens, the drift occurs as per the ACI 374.1-05 loading pattern, starting from 0% drift to maximum drift where the column has collapsed. As a result of this drift, the vertical fibers on the left and right sides of the test specimens changed their orientation following the drift, this change must be measured properly. This measurement is useful as a basis for measuring and calculating the amount of curvature for each phase of the tensile-compressive test. If it has gone through the push-pull phase 3 times, this is called one (1) cycle according to ACI 374.1-05 Reapproved 2014. Good curvature measurements are of course influenced by good measuring instruments, in this case, an LVDT (linear variable displacement transducers) measuring instrument is used which is capable of supplying data in the thousandths of an mm. However, the accuracy of the location of the LVDT tool also greatly determines the purpose of the measurement, for this reason, the location of the measurement device was designed as shown in Figure 6.

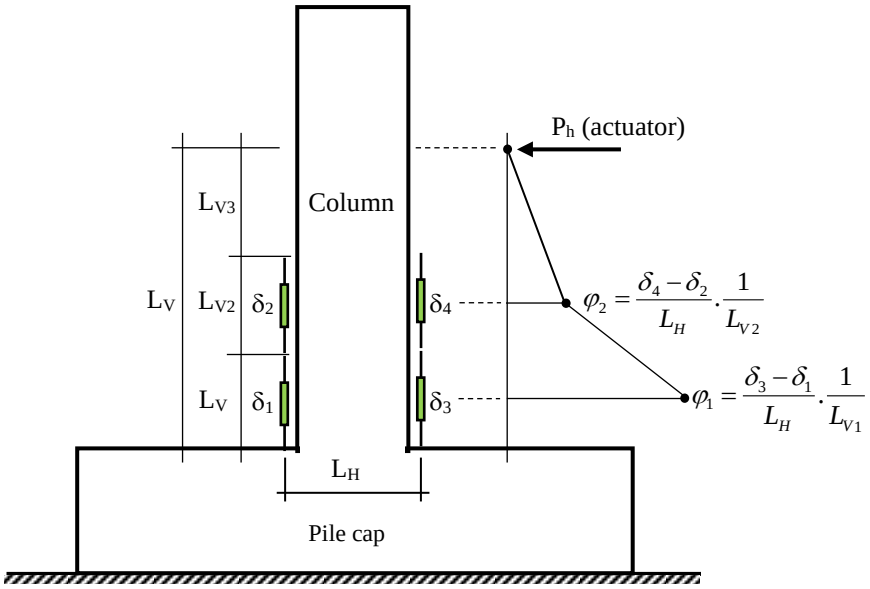

Figure 6. Location of LVDTs and calculation of column curvature based on LVDT data, value δ_1 = LVDT measurement result no. 5, δ_2 = LVDT measurement result no. 6, δ_3 = LVDT measurement result no. 7 and δ_{14} = LVDT measurement result no. 8, while φ_1 and φ_2 are the curvature values [47].

2.5. Test Setup

The most important part of the column test is the assembly of all the devices to measure the test data which includes the magnitude of the load $P_{h\text{-}lateral}$, the load $P_{constant\text{-}axial}=0.121.A_g.f'_c$, and the magnitude of the drift ratio. This circuit must be precise such that the measurement results are valid. Column testing used the displacement control method. This method is in perfect accordance with ACI 374.1-05 rules (see Figure 7). However, this series also adapts to the testing laboratory conditions. Without reducing the need for test results, a test setup was created based on the development of Figure 6. The actual test setup is also shown in Figure 8.

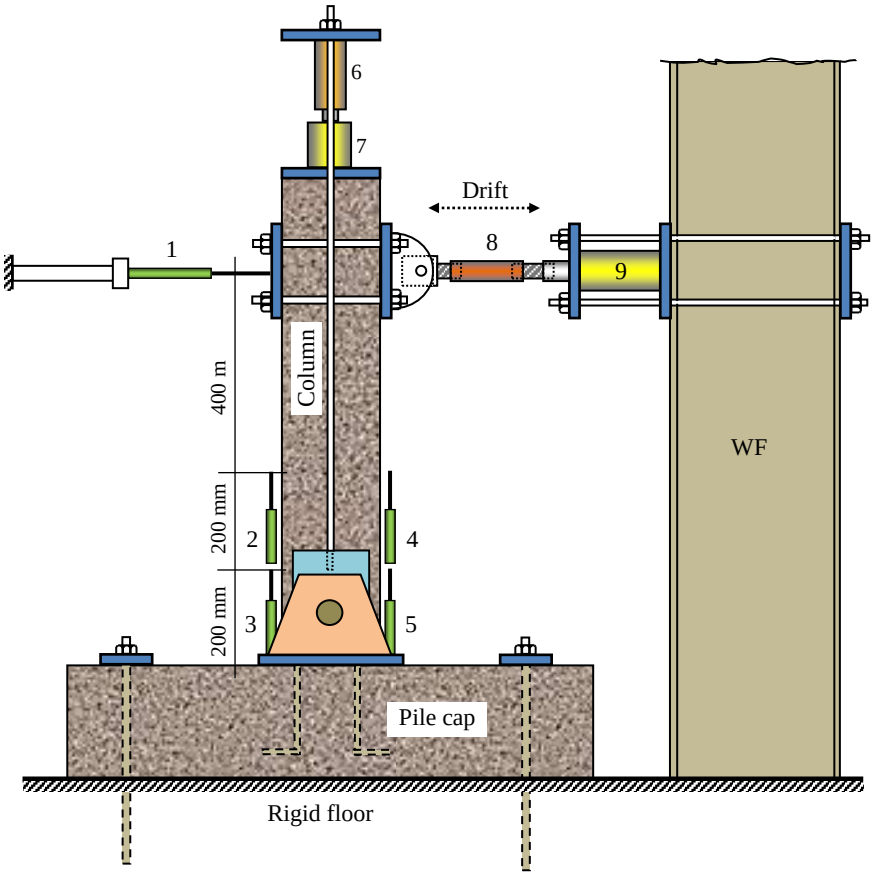

Figure 7. The setup schematic above is adapted to laboratory conditions, 1-5 = LVDT, 6 = hydraulic Jack-single acting, 7 = load cell-single acting, 8 = load cell-double acting, 9 = hydraulic Jack-double acting, ⟷ = quasi-cyclic load direction

Figure 8. Actual test setup and drift occurred during testing

2.6. Test Drift

The amount drift ratio is calculated based on the ratio of the amount of drift to the height of the column and then converted into column displacement as in Table 10 and Figure 9. This table is used as a displacement-controlled reference.

Table 10. Drift ratio for all columns, L_{column} = 800 mm

Cycle #	Drift ratio (%)	Displacement (mm)
1	0.20	1.60
2	0.25	2.00
3	0.35	2.80
4	0.50	4.00
5	0.75	6.00
6	1.00	8.00
7	1.40	11.20
8	1.75	14.00
9	2.20	17.60
10	2.75	22.00
11	3.50	28.00
12	4.38	35.00
13	5.47	43.75
14	6.84	54.69
15	8.54	68.36
16	10.68	85.45

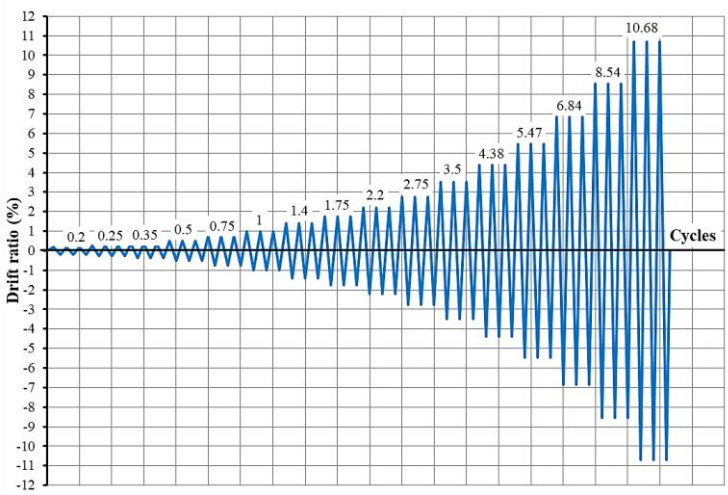

Figure 9. Displacement controlled loading pattern

3. Results and Discussions

3.1. Curvature measurement results

The measurement of column curvature is appropriate using the displacement control testing method, namely that the column is treated/given displacement according to Table 10 which has been converted to displacement (mm). Displacement is given starting from 0 and stopped until the column has reached failure, or the displacement is stopped after reaching more than 80%P_{max}. Then the relationship between the curvature and the magnitude of the moment that occurs is described. The conditions describe quasi-cyclic loading so that the load and curvature can be seen when the column is subjected to compressive and tensile forces, as well as the curvature conditions when it receives compressive and tensile forces.

3.2. Plastic Hinge Length Analysis

Based on the maximum curvature (φ) of each phase at each value of φ_1 and φ_2, the relationship between column height and curvature was then described. In this case, the curvature in question is the maximum curvature of each quasi-cyclic phase. The quasi-cyclic test was carried out with a push-pull controlled displacement pattern (see Table 10)

starting from 0 to the maximum displacement of each test specimen. Each displacement that occurred affected the curvature values φ_1 and φ_2. The length of the plastic hinge was obtained based on the relationship of each compression-tension curvature vs. column height. More precisely, they were measured at the locations of the curvature measuring instruments (see Figure 6). The midpoint positions φ_1 and φ_2 are located at the midpoint of the height of $LVDT_1$ = 100 mm, $LVDT_3$ = 100 mm, $LVDT_2$ = 300 mm, and $LVDT_4$ = 300 mm. This relationship is depicted in Figures 10 to 24. Applying several existing theories, the plastic hinge length l_P is obtained based on the relationship between curvature and column height.

Figures 10 to 24 are the results of experimental analysis of the length of plastic hinges for each test column specimen based on the quasi-cyclic test. The red line in Figures 10 to 24 represents the rotation of the first compression and tension yield curvature, while the dotted red line represents the maximum compression and tension curvature. The two images of the top-bottom green triangle are the result of trial and error, where the results must show two triangles that have the same area. The height of one of the triangles represents the length of the plastic hinge (l_p), both l_p compression ($l_{p\text{-}exp\text{-}compression}$) and l_p tension ($l_{p\text{-}exp\text{-}tension}$). Then the average value was calculated from the two l_p and the results were compared with the $l_{p\text{-}proposed}$. The l_p length obtained based on trial data for each test specimen turned out to be slightly different, and they were still in the range of 92.80-100.25 mm (see Table 11). From further observation, the results of this research indirectly strengthened the statement that determining the length of plastic hinges is problematic and complicated. These obstacles and complexities are mainly due to the nonlinear behavior of the materials [11]. However, in this study, a trend was still found (see Figures 25) due to the use of different s_h and V_f. The trend shows that as a result of using s_h, the wider the l_p, the longer it is, conversely, the more volumetric V_f causes the l_p to be shorter. The results of these two different trends are what causes the plastic hinge length $l_{p\text{-}all.average}$ to be controlled in the range of 97.03 mm (see Table 11). However, if the observed results of the $l_{p\text{-}average}$ for each test specimen are compared to $l_{p\text{-}all.average}$, the results indicate that the difference only ranges between 0.11% - 4.36% (see Table 11), meaning that there is not much difference in the l_p between the test specimens.

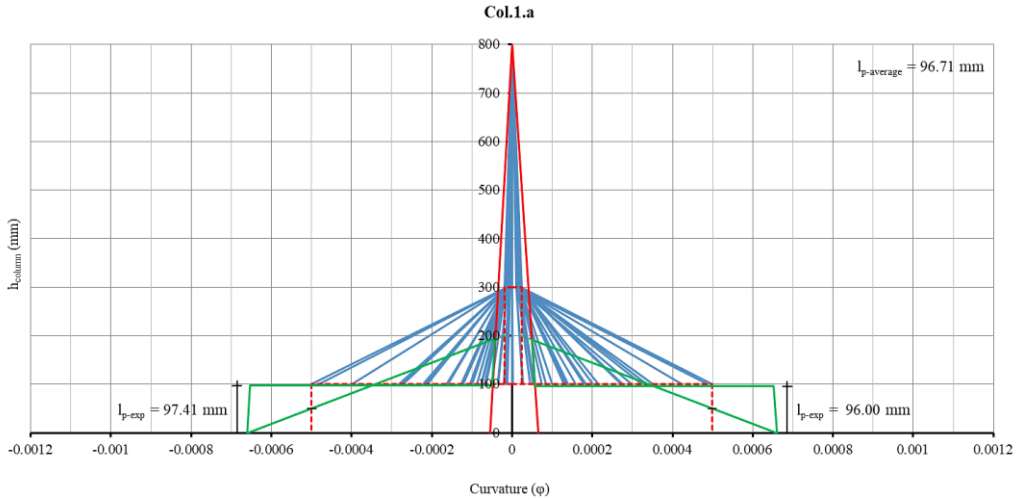

Figure 10. Length of l_p of column Col.1.a

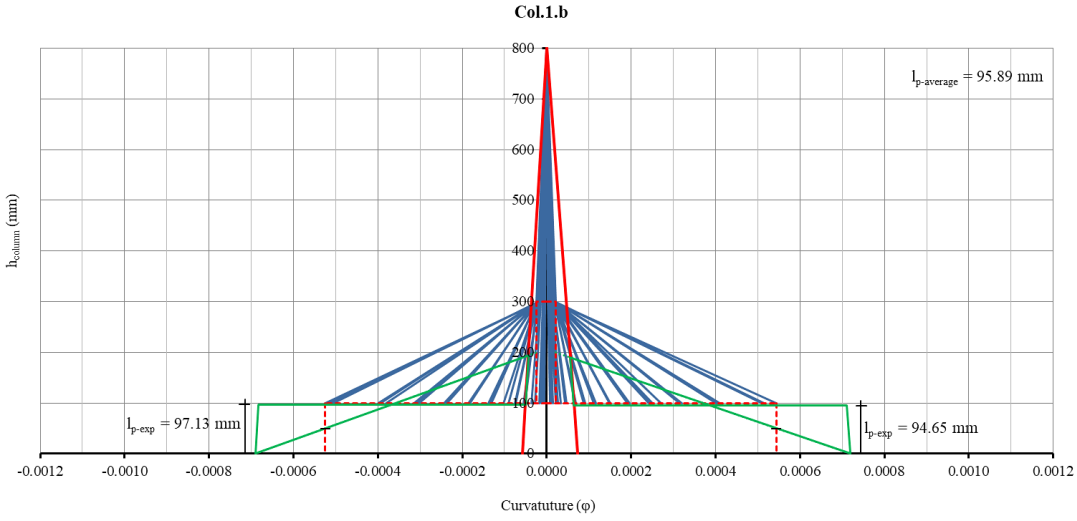

Figure 11. Length of l_p of column Col.1.b

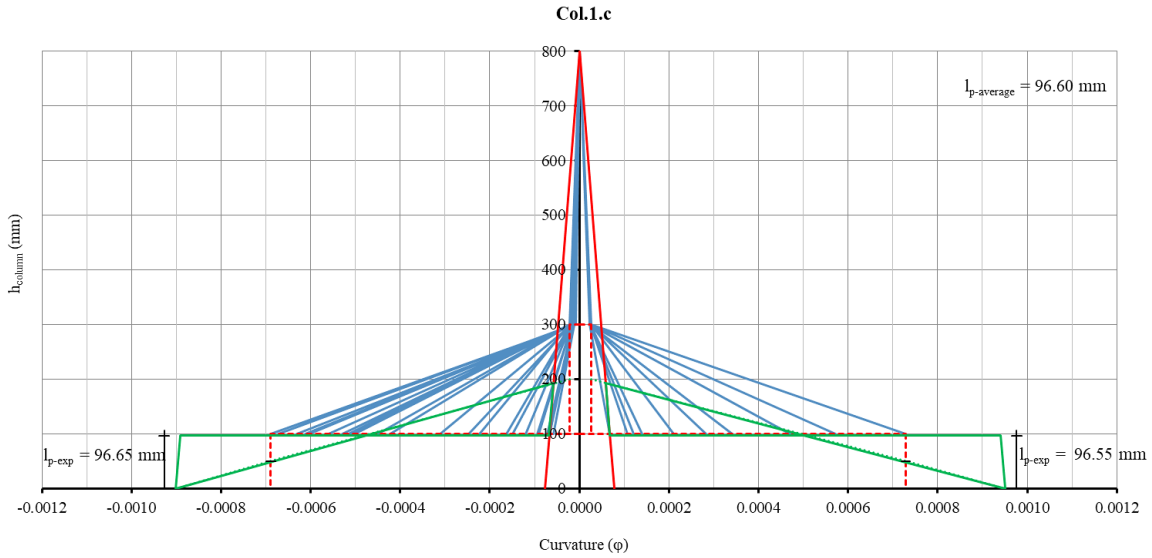

Figure 12. Length of l_p of column Col.1.c

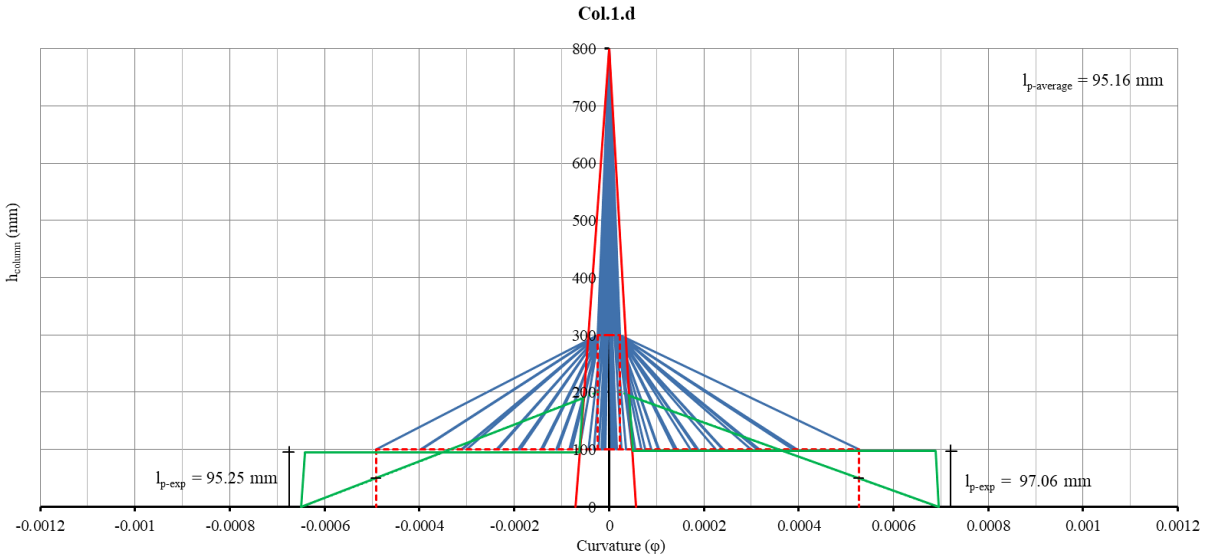

Figure 13. Length of l_p of column Col.1.d

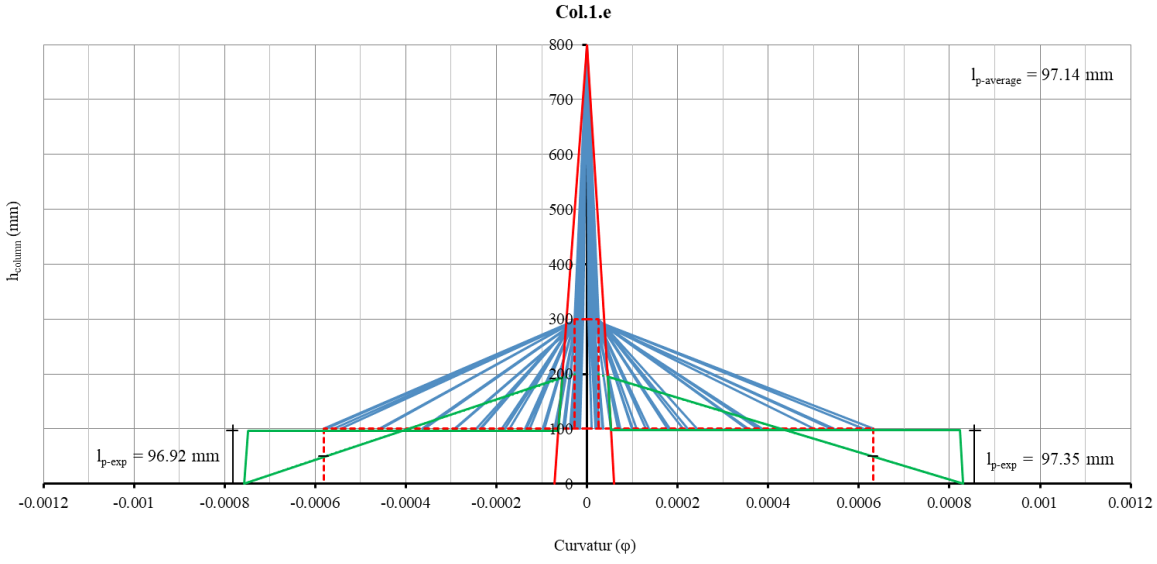

Figure 14. Length of l_p of column Col.1.e

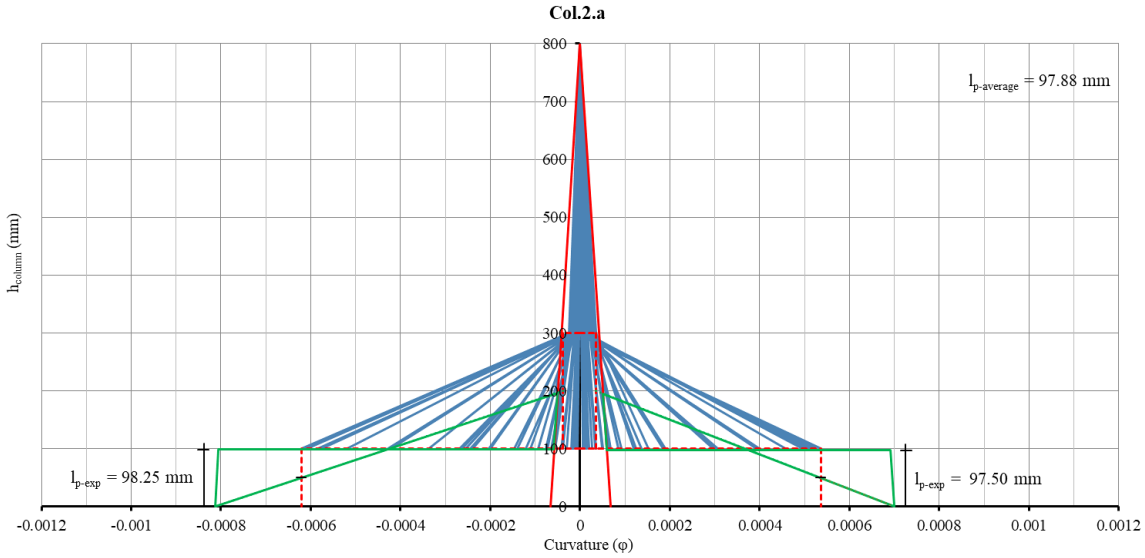

Figure 15. Length of lp of column Col.2.a

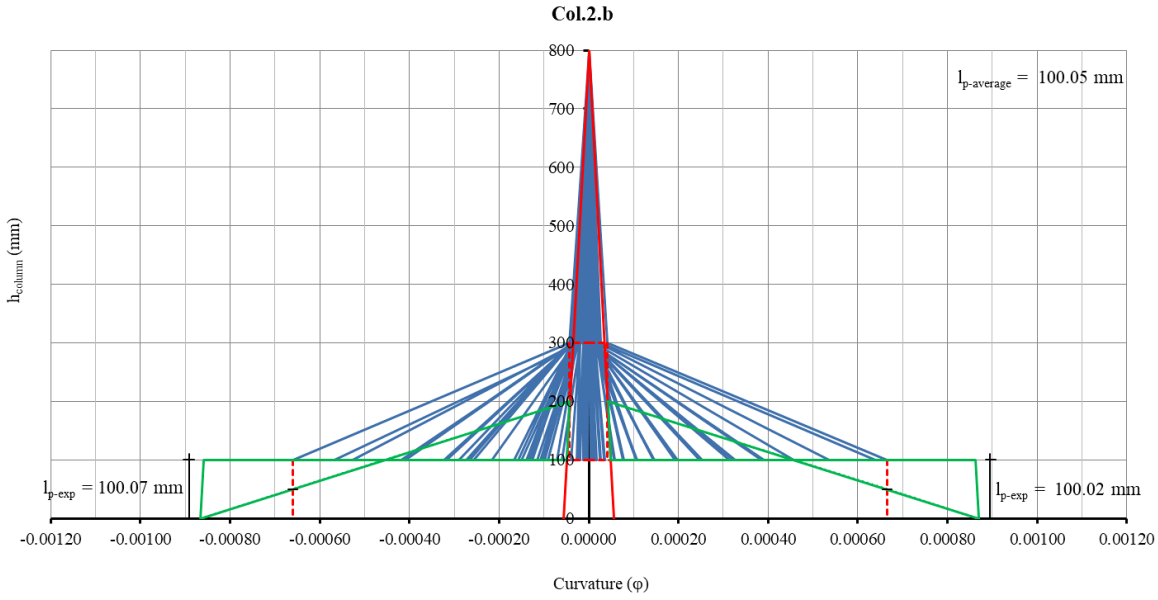

Figure 16. Length of l_p of column Col.2.b

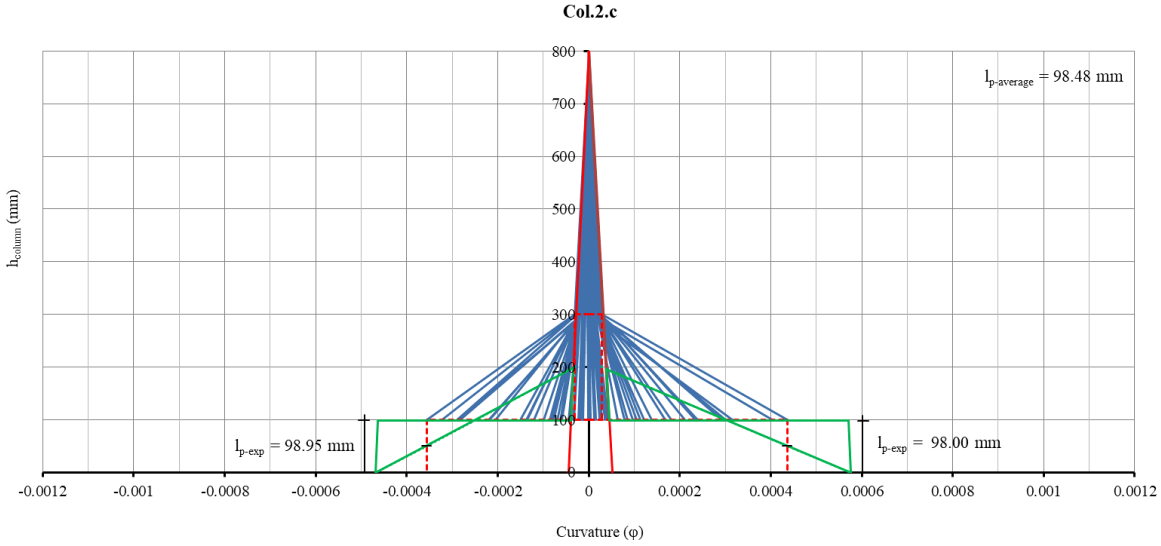

Figure 17. Length of l_p of column Col.2.c

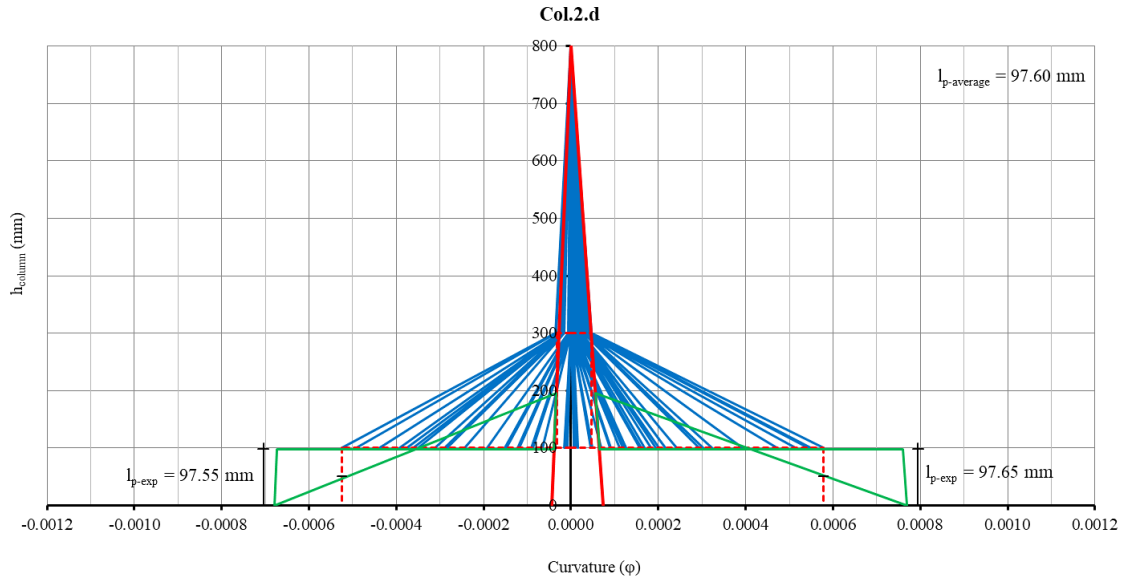

Figure 18. Length of l_p of column Col.2.d sh=65 vf=1.5%

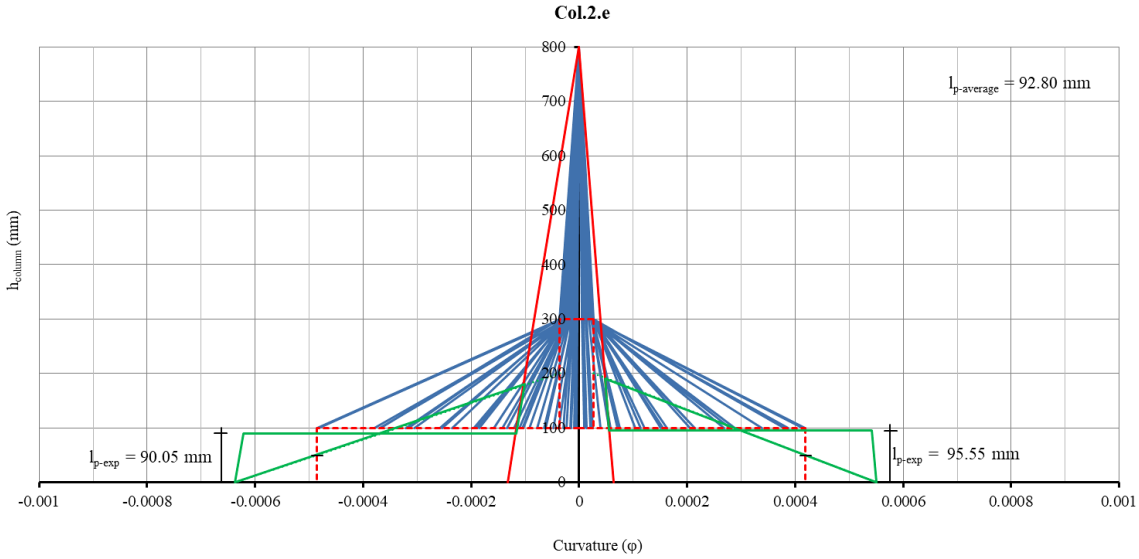

Figure 19. Length of l_p of column Col.2.e

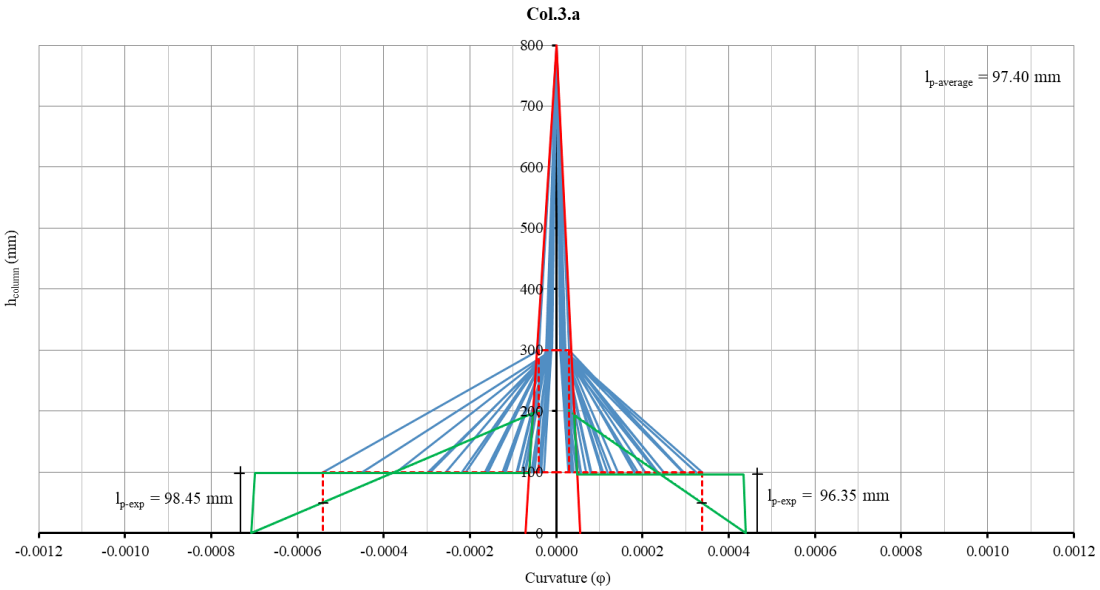

Figure 20. Length of l_p of column Col.3.a

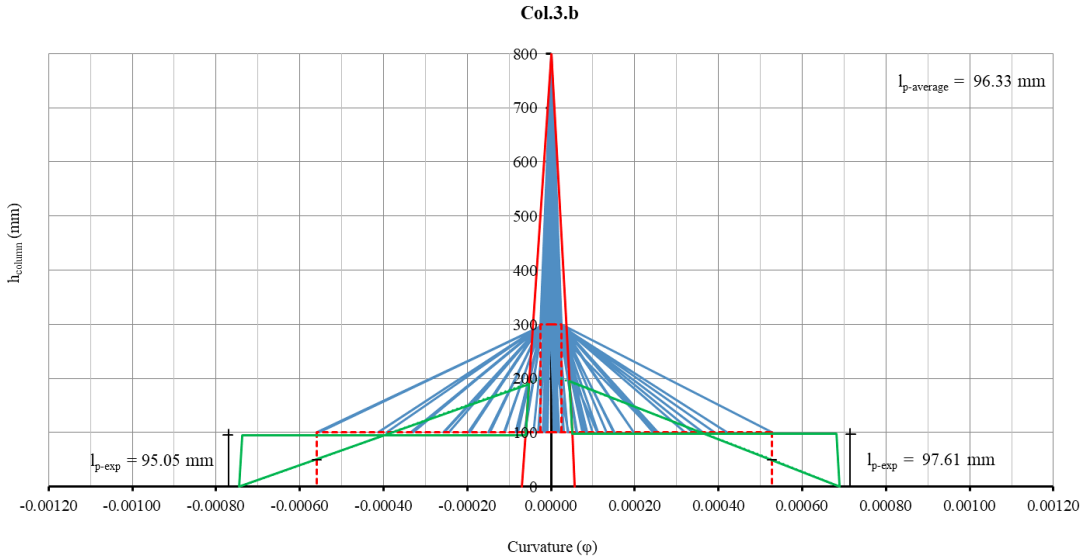

Figure 21. Length of l_p of column Col.3.b

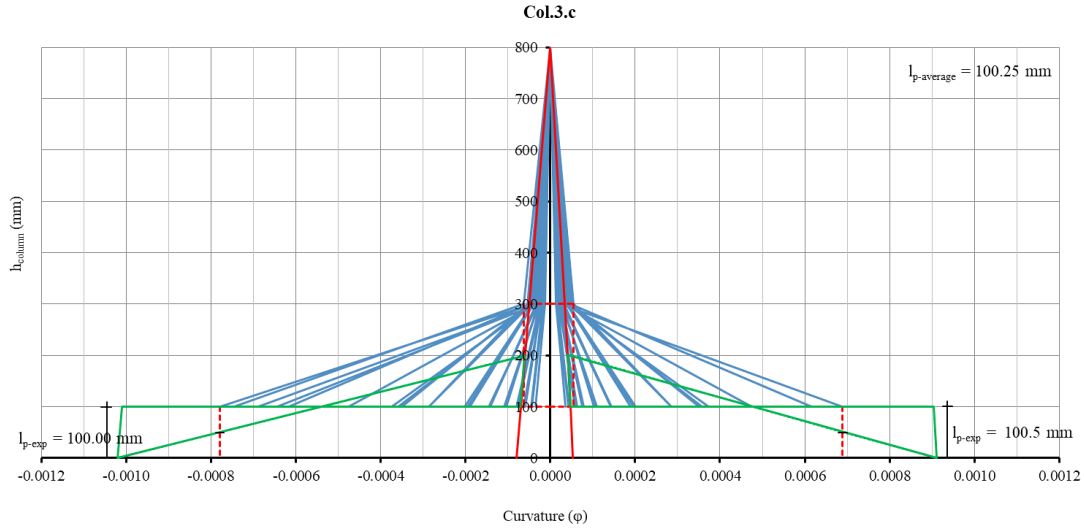

Figure 22. Length of l_p of column Col.3.c

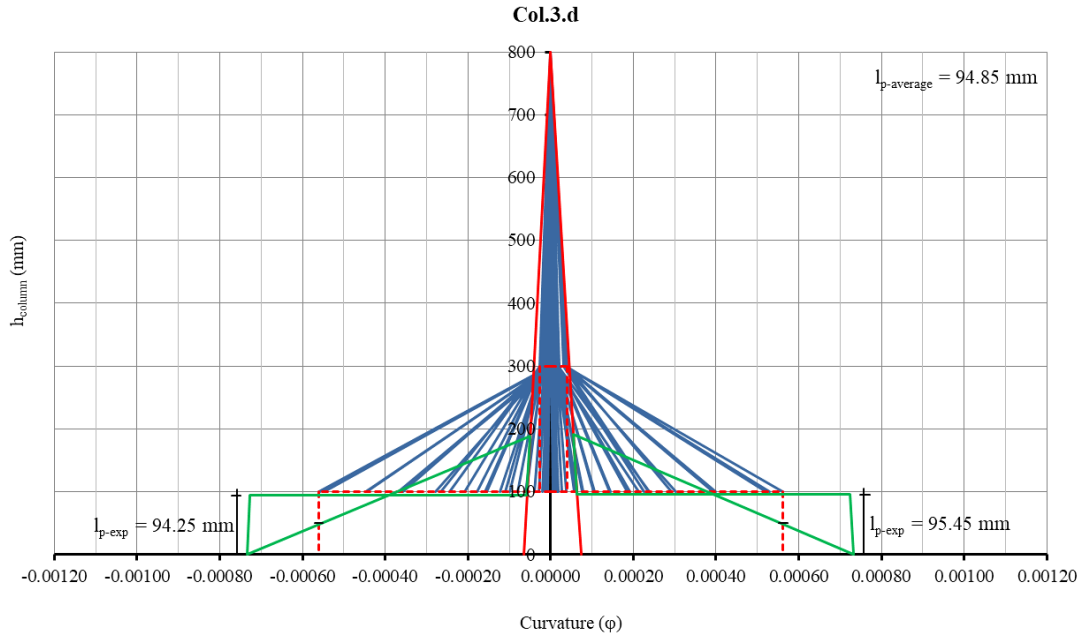

Figure 23. Length of l_p of column Col.3.d

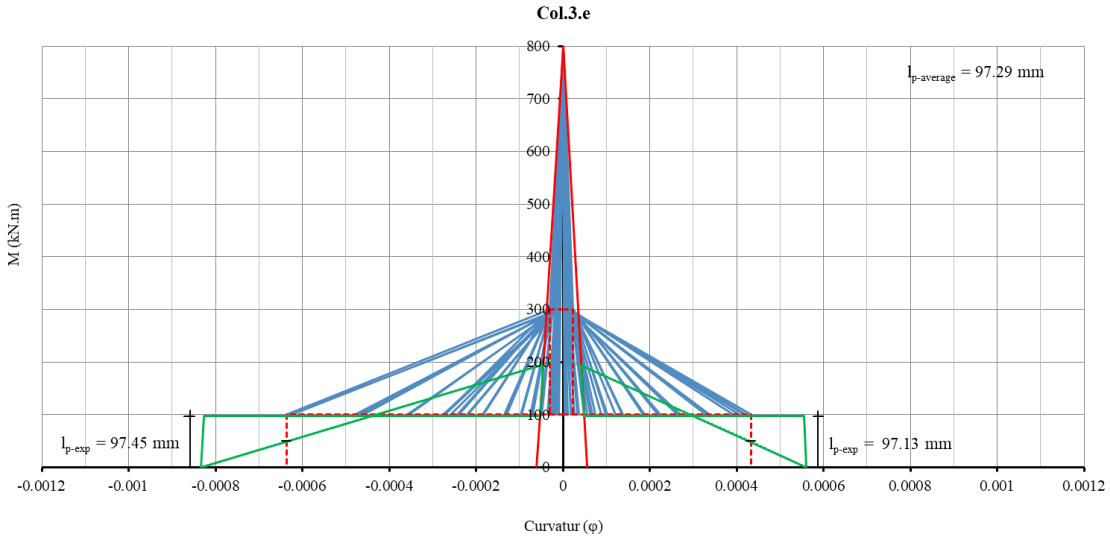

Figure 24. Length of l_p of column Col.3.e

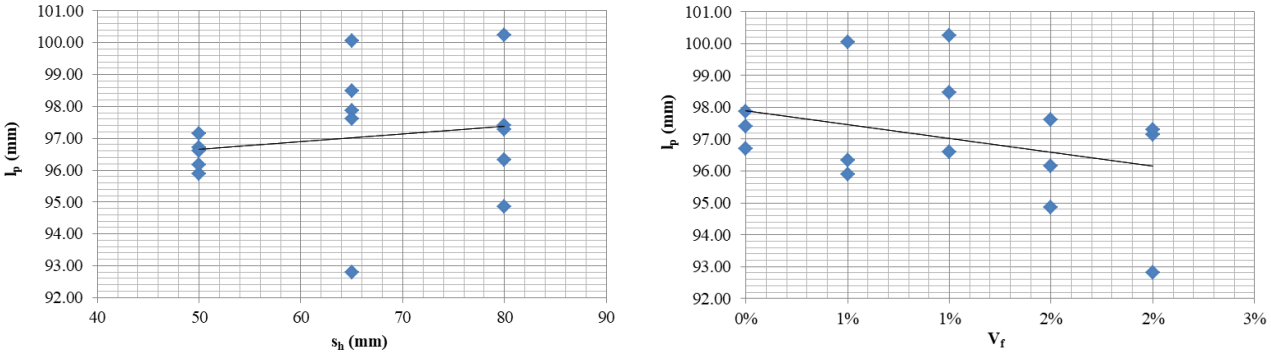

(a) (b)

Figure 25. Relationship of s_h vs l_p dan V_f vs l_p

Table 11. Difference between $l_{p\text{-proposed}}$ and $l_{p\text{-exp. average}}$

No.	Specimen ID	V_f	P/P_o	A_s/A_g	f'_{ccf}/f'_c	C	h_{column} (mm)	$l_{p\text{-prop}}$ (mm)	$l_{p\text{-exp.average}}$ (mm)	Difference $l_{p\text{-exp.average}}$ vs $l_{p\text{-pro}}$ (%)	Ratio $l_{p\text{-exp.average}}$ to $l_{p\text{-all.average}}$ (%)
1	Col.1.a	0%	0.0901	0.0248	1.193	0.390	200	102.02	96.71	5.21	0.33
2	Col.1.b	0.5%	0.0901	0.0248	1.136	0.415	200	103.79	95.89	7.61	1.17
3	Col.1.c	1%	0.0901	0.0248	1.192	0.414	200	108.31	96.60	10.81	0.44
4	Col.1.d	1.5%	0.0901	0.0248	1.104	0.389	200	94.75	96.16	1.48	0.90
5	Col.1.e	2%	0.0901	0.0248	1.445	0.338	200	105.31	97.14	7.76	0.11
6	Col.2.a	0%	0.0901	0.0248	1.112	0.390	200	95.67	97.88	2.30	0.87
7	Col.2.b	0.5%	0.0901	0.0248	1.070	0.415	200	98.31	100.05	1.76	3.11
8	Col.2.c	1%	0.0901	0.0248	1.094	0.414	200	100.23	98.48	1.75	1.49
9	Col.2.d	1.5%	0.0901	0.0248	1.039	0.389	200	89.76	97.60	8.73	0.59
10	Col.2.e	2%	0.0901	0.0248	1.327	0.338	200	97.33	92.80	4.65	4.36
11	Col.3.a	0%	0.0901	0.0248	1.065	0.390	200	92.04	97.40	5.82	0.39
12	Col.3.b	0.5%	0.0901	0.0248	1.043	0.415	200	96.06	96.33	0.28	0.72
13	Col.3.c	1%	0.0901	0.0248	1.054	0.414	200	96.91	100.25	3.45	3.32
14	Col.3.d	1.5%	0.0901	0.0248	1.013	0.389	200	87.71	94.85	8.14	2.24
15	Col.3.e	2%	0.0901	0.0248	1.278	0.338	200	94.05	97.29	3.44	0.27
							All-average		97.03	4.88	

Note Col.1= s_h 50 mm, Col.2= s_h 65 mm, Col.3= s_h 80 mm, a=V_f 0%, b=V_f 0.5%, c=V_f 1%, d=V_f 1.5%, e=V_f 2%.

3.3. Proposed Plastic Hinge Length Equation

The proposed plastic hinge length (l_p) applies the Buckingham Pi Theorem [48]. The Buckingham method is a method for determining dimensionless numbers. Therefore, tracking the proposed plastic length uses this theory because almost all plastic hinge length formulas tend to be non-dimensional, but solving the l_p formula produces dimensions of unit length. Several parameters considered to determine l_p are arranged in Table 12. The preparation of the table follows the pattern of Buckingham's theory by bringing up the units and writing the dimensions, where the dimension M is related to mass (weight, force) in units of N (Newtons), L is related to length in units. units are mm, and T is related to time in units of time (seconds).

The discussion on l_p is intended to develop the l_p theoretical equations of Bae & Bayrak [49] and l_p based on Ou et al. [50]. The repeating parameters are taken P_o, A_s, and P_h so these parameters must be simplified, they must have dimensions, but must not have the same dimensions. The combination of the three is the main dimension, and the three must not form a dimensionless variable, and the repeated parameters must have complete dimensions, namely M, L, and T. The selection of parameters in Table 12 is due to gaps in the l_p formula of other researchers who have not included steel fiber parameters and several determining parameters in quasi-cyclic testing. The steel fiber parameters have been accommodated in the f'_{ccf} value [43].

Table 12. Parameters considered influence of the plastic hinge length

Variables	P_o	f'_c	P_h=F	P_a	f'_{ccf}	l_p	A_g	A_s	h
Unit	N	N/mm^2	N.m/dt^2	N	N/mm^2	mm	mm^2	mm^2	mm
Dimension	M	ML^{-2}	MLT^{-2}	M	ML^{-2}	L	L^2	L^2	L
M	1	1	1	1	1	0	0	0	0
L	0	-2	1	0	-2	1	2	2	1
T	0	0	-2	0	0	0	0	0	0

The test column specimens were assigned with a horizontal load P_h as a quasi-cyclic load per ACI 374.1-05 Reapproved 2014. This P_h represents the earthquake force, while the earthquake force itself is $F = m.a$, where F is the internal force due to the external force m in the form of mass (N) and a is the earthquake acceleration (m/s^2), so P_h is analogous to $F = m.a$. From the experimental tests, it can be obtained the values of compression, tension, and average of $l_{p\text{-}exp}$. Thus, the values of $l_{p\text{-}exp.average}$ in Table 11 are given by the $l_{p\text{-}exp.average}$ obtained in Table 13.

Table 13. Recapitulation of $l_{p\text{-}exp}$ from test results

No.	Specimen ID	$l_{p\text{-}exp}$ compression (mm)	$l_{p\text{-}exp}$ tension (mm)	$l_{p\text{-}exp.average}$ (mm)
1	Col.1.a	97.41	96.00	96.71
2	Col.1.b	97.13	94.65	95.89
3	Col.1.c	96.65	96.55	96.60
4	Col.1.d	95.25	97.06	96.16
5	Col.1.e	96.92	97.35	97.14
6	Col.2.a	98.25	97.50	97.88
7	Col.2.b	100.07	100.02	100.05
8	Col.2.c	98.95	98.00	98.48
9	Col.2.d	97.55	97.65	97.60
10	Col.2.e	90.05	95.55	92.80
11	Col.3.a	98.45	96.35	97.40
12	Col.3.b	95.05	97.61	96.33
13	Col.3.c	100.00	100.50	100.25
14	Col.3.d	94.25	95.45	94.85
15	Col.3.e	97.45	97.12	97.29

The parameters mentioned above are a logical simplification based on the Buckingham P_i Theorem, but the development is based on two formulas that include column axial (P_a) in the research, including:

- Plastic hinge length l_p according to Bae and Bayrak [49]:

This formula has developed a hinge length formula based on the following column axial (P_a) values:

$$\frac{lp}{h} = \left[0.3\left(\frac{P}{P_o}\right) + 3\left(\frac{A_s}{A_g}\right) - 0.1\right]\left(\frac{L}{h}\right) + 0.25 \geq 0.25 \quad (1)$$

- Plastic hinge length l_p according to Ou et al. [50];

The development of the formula is based on:

1. Main reinforcement with yield strength = 414 MPa and f '$_c$ units in MPa:

$$\frac{lp}{h} = 0.936\left(\frac{P}{P_o}\right) + 7.398\left(\frac{A_s}{A_g}\right) + 0.06\left(\frac{L}{h}\right) - 0.003(f'_c) \quad (2)$$

2. Main reinforcement with yield strength = 685 MPa and f'$_c$ units in MPa

$$\frac{lp}{h} = 0.503\left(\frac{P}{P_o}\right) + 3.218\left(\frac{A_s}{A_g}\right) + 0.053\left(\frac{L}{h}\right) + 0.0018(f'_c) \quad (3)$$

where h=column cross-sectional depth, P=column axial force, P_0=0.85.f'$_c$.(A_g–A_s)+f_y.A_s= nominal axial force, A_s=column reinforcement area, A_g=gross concrete cross-sectional area, L=column length.

Steps to simplifying several parameters in Table 12 above by taking the repeated parameters are P_o, f′$_{ccf}$, F so that several values π_i up to π_n values that the calculated value π_i up to π_n values can be obtained as follows:

$$\pi_1 = \frac{f'_c.A_s}{P_0}, \pi_2 = \frac{f'_c.A_g}{P_0}, \pi_3 = \frac{\sqrt{P_o}.l_p}{\sqrt{f_{ccf}}}, \pi_4 = \frac{\sqrt{P_o}.h}{\sqrt{f'c}}, \pi_5 = \frac{P_a}{P_o}, and\ \pi_6 = \frac{f'_{ccf}}{f'_c} \quad (4)$$

Some of the π values mentioned above are simplified again with the aim of all π values being non-dimensional. In this case, the simplification is also attempted to approach the formula that has been developed by Bae and Bayrak and Ou et al. The simplification concept of the Buckingham *Pi Theorem* is by multiplying, dividing, adding, or subtracting between π, the solution and the results are given in Table 14.

Table 14. Simplification of π value

Simplified π_1 s/d π_6	Note
$\pi_5 = \frac{P_a}{P_o}, \pi_6 = \frac{f'_{ccf}}{f'_c}$	non-dimensional
$\pi_7 = \frac{\pi_1}{\pi_2} = \frac{\left(\frac{f'_c.A_s}{P_o}\right)}{\left(\frac{f'_c.A_g}{P_o}\right)} = \frac{A_s}{A_g}$	non-dimensional
$\pi_8 = \frac{\pi_3}{\pi_4} = \frac{\left(\frac{\sqrt{P_o}.l_p}{\sqrt{f'_c}}\right)}{\left(\frac{\sqrt{P_o}.h}{\sqrt{f'_c}}\right)} = \frac{l_p}{h}$	

Thus, the value π in Table 14 can be rearranged as follows:

$$f(\pi_5,\ \pi_6,\ \pi_7,\ \pi_8) = f(\frac{P_a}{P_o},\ \frac{f'_{ccf}}{f'_c},\ \frac{A_s}{A_g},\ \frac{l_p}{h}) = 0 \quad (5)$$

$$atau \rightarrow f(\pi_5,\ \pi_6,\ \pi_7,\ \pi_8) = f(\frac{P_a}{P_o},\ \frac{A_s}{A_g},\ \frac{f'_{ccf}}{f'_c},\ \frac{l_p}{h}) = 0 \quad (6)$$

Meanwhile, the solution to the function equation π is:

$$l_p = C.(\frac{P_a}{P_o} + \frac{A_s}{A_g} + \frac{f'_{ccf}}{f'_c}).h \quad (7)$$

Equation 7 has a non-dimensional form and is close to the Bae and Bayrak equation [49] and the equation of Ou et al. [50], but differs in the value of the constant C, where the value of C affects all non-dimensional parameters. After obtaining the constant C, it is then validated based on the experimental results of the plastic hinge length and also validated/compared with other l_p equations (see Figure 26). Meanwhile, the f'$_{ccf}$ value is used by the equation from Sabariman et al. [43].

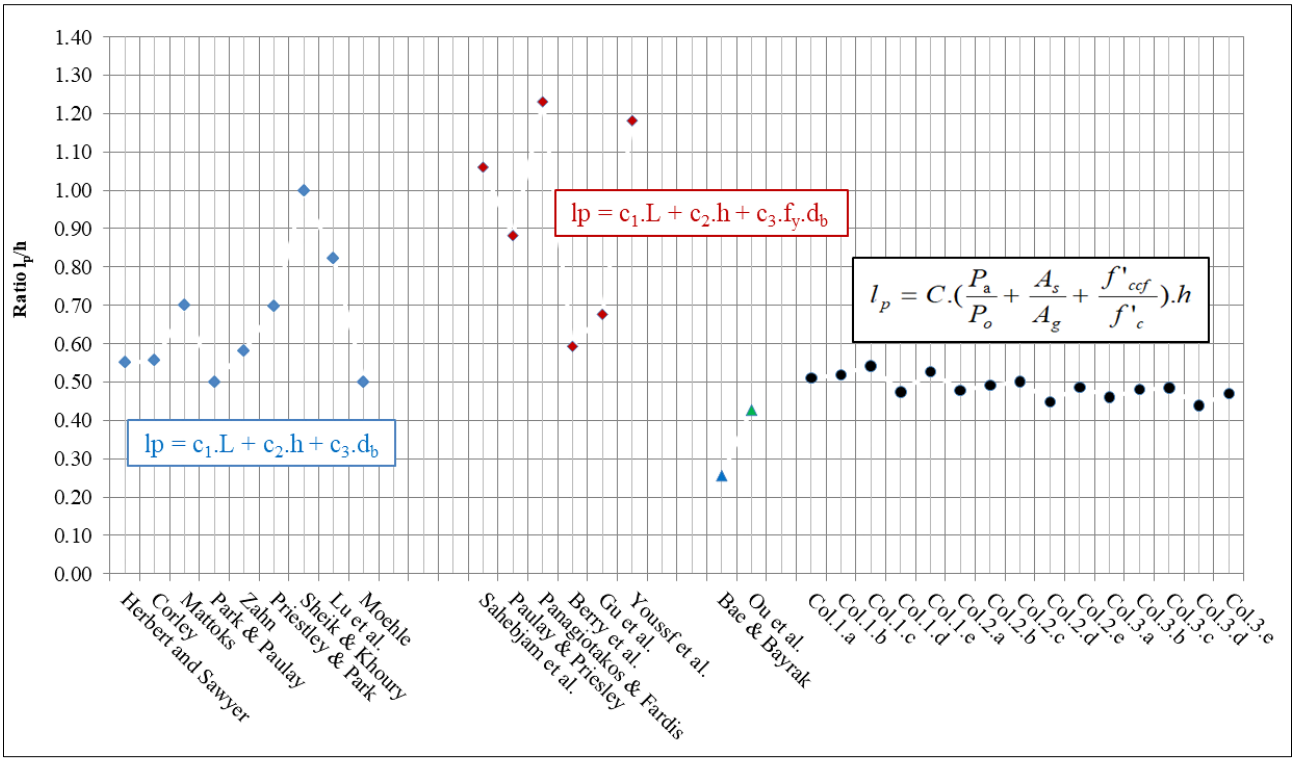

Figure 26. Description of l_p/h ratio based on the three basic plastic hinge length formulas, C, c_1, c_2, c_3 = constant

3.4. Coefficient C

The calculation of the C coefficient value is obtained based on the interaction between the values in Table 11 and Equation 7. After all the C values have been obtained, they are then included in the graph of the relationship between V_f and C to see the trend. The graphic regression trend is shown in Figure 27.

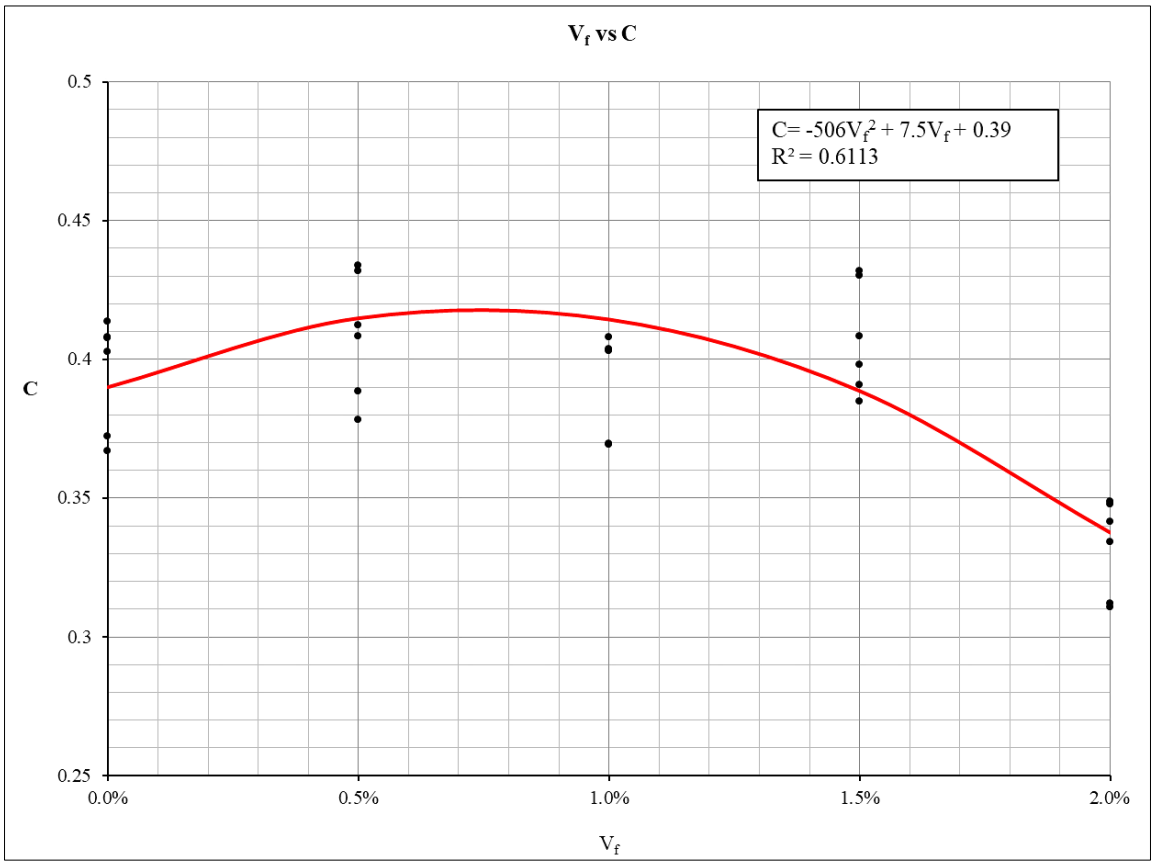

Figure 27. C coefficient value supports the proposed Equation 7

Based on the regression trend in Figure 27, the value of C is taken as $C = -506V_f^2 + 7.5V_f + 0.39$, then the proposed Equation 7 and the value of C were validated against the l_p results of the experimental analysis. The validation results showed that the proposed l_p formula only had a small difference, namely 4.88% < 5% (see Table 11). The validation results are shown in Table 11. As a comparison of several plastic hinge length formulas such as Sahebjam [13], Herbert & Sawyer [14], Corley [15], Mattoks [16], Park & Paulay [17], Zahn [18], Priestley and Park [19], Sheik and Khoury [20], Lu et al. [21], Moehle [22], Paulay & Priestley [23], Panagiotakos & Fardis [24], Berry et al. [25], Gu et al. [26] and Youssf et al. [27] is depicted in Figure 26. Figure 26 is based on three groups of plastic hinge length formulas and shows the proposed formula l_p under conservative conditions. This is per the condition of the column specimen; the damage tends to be due to bending damage. The length of plastic hinges due to bending tends to be shorter than the length of plastic hinges due to shear damage.

3.5. Ductility and Crack Pattern

This experiment also physically observed damage around the long area (test area), damage to all test specimens tended to be due to bending damage, which was per previous design predictions, where FSSR < 0.6 was taken. In this study, it was also seen that the lengths of the plastic hinges of all test specimens were not greater than 0.5h of the column cross-section. Bae & Bayrak [49] illustrate that the influence of the magnitude of the P_{axial} level influences the length of the plastic hinge, the greater the P_{axial}, the longer the plastic hinge formed. However, in this study the average l_p = 97.03 mm is not more than half of h (see Table 11), and the results are relatively short. This is also suspected to be due to $P_{axial} = 0.121.A_g.f'_c$ (axial is relatively small) and corresponds to the designed FSSR value < 0.6. This small axial impact causes all of the test specimens to be damaged due to bending. This research also found that all test specimens behaved in a very ductile manner because all the ductility values were $\mu_\Delta > 4$ (Table 15 and Figure 28).

Table 15. Ductility of test specimens

Group of Specimens	μ_Δ	Criteria based on the Federal Emergency Management Agency (FEMA) [37]
$C_{50,0} - C_{50.2}$	5.14 - 10.60	Highly ductile
$C_{65,0} - C_{65.2}$	4.02 - 15.95	Highly ductile
$C_{80,0} - C_{80.2}$	4.00 - 13.27	Highly ductile

(a) Specimen Col.1.a

(b) Specimen Col.1.b

(c) Specimen Col.1.c

(d) Specimen Col.1.d

(e) Specimen Col.1.e

(f) Specimen Col.2.a

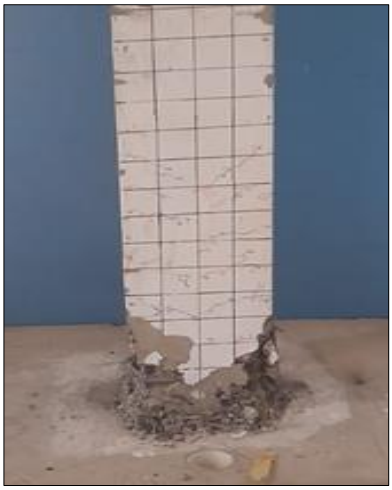

(g) Specimen Col.2.b

(h) Specimen Col.2.c

(i) Specimen Col.2.d

(j) Specimen Col.2.e

(k) Specimen Col.3.a

(l) Specimen Col.3.b

(m) Specimen Col.3.c

(n) Specimen Col.3.d

(o) Specimen Col.3.e

Figure 28. Damage Patterns of Column Specimens

4. Conclusion

In laboratory experiments, the ductility of reinforced concrete column structures can be analyzed based on the displacement that occurs, namely the ultimate displacement divided by the displacement at first yield, but, apart from measuring displacement, curvature that occurs along the vertical fibers of the column can also be measured. This curvature measurement can be used as a guide for measuring column plastic hinges because there is a relationship between the curvature formed and the length of the plastic hinge. However, the axial load of the column is also related to the length of the plastic hinge, the greater the axial column, the longer the plastic hinge of the column.

Research on steel fiber in reinforced columns can also increase column ductility, especially post-peak load ductility, namely at the condition of $0.8P_{max}$. In this research, using steel fiber in reinforced concrete columns has shown high ductile results, which were obtained $\mu_{\Delta} > 4$. As a result of using $P_{axial} = 0.121.A_g.f'_c$, according to predictions, the damage tends to be due to damage due to bending in the plastic hinge area. Even though the bending damage collects in the plastic hinge area, it is still necessary to know the length of the plastic hinge, especially since this study used steel fiber in its research. The proposed plastic hinge length formula in this study has considered the axial load ratio, longitudinal reinforcement area ratio, and influence ratio of steel fiber usage.

5. Declarations

5.1. Author Contributions

Conceptualization, T.; methodology, T.; software, B.S.; validation, B.S. and S.W.; investigation, S.W.; data curation, B.S.; writing—original draft preparation, B.S.; writing—review and editing, T.; supervision, T. All authors have read and agreed to the published version of the manuscript.

5.2. Data Availability Statement

The data presented in this study are available on request from the corresponding author.

5.3. Funding

The authors express their sincere gratitude for all the funding received from the 2023 Indonesian Collaborative Research grant, under ITS with contract no. 1662/PKS/ITS/2023, UNESA with contract no. B/38242/UN38.III.1/LK.04.00/2023, and UNY with contract no. T/9.1.8 /UN/34.9/PT.01.03/2023. The authors also gratefully acknowledge the financial support received from the Institut Teknologi Sepuluh Nopember for this work, under the project scheme of the Publication Writing and IPR Incentive Program (PPHKI) 2023.

5.4. Acknowledgements

The researcher acknowledges that this research can be achieved with the financial support of Internal Grants from ITS, UNESA, and UNY.

5.5. Conflicts of Interest

The authors declare no conflict of interest.

6. References

[1] CDP. (2023). Turkey-Syria Earthquake 2023. Center for Disaster Philanthropy, Washington, United States. Available online: https://disasterphilanthropy.org/disasters/2023-turkey-syria-earthquake/ (accessed on April 2024).

[2] Rakaa, I. G. P., Tavio, & Astawaa, M. D. (2014). State-of-the-art report on partially-prestressed concrete earthquake-resistant building structures for highly-seismic region. Procedia Engineering, 95, 43–53. doi:10.1016/j.proeng.2014.12.164.

[3] ACI 318-19 (2019). Building Code Requirements for Structural Concrete, American Concrete Institute, Michigan, United States.

[4] Christianto, D., Tavio, & Irianto, M. R. (2023). Shear Strength of SFRC Beams Without Coarse Aggregate Using Finite Element Analysis with Bond-Slip. International Review of Civil Engineering, 14(4), 320–330. doi:10.15866/irece.v14i4.22482.

[5] Honestyo, A., Tavio, & Ardhyananta, H. (2023). Axial Compressive Behavior of Bubble-Size Plastic Straw Waste FRP-Confined Circular Concrete. International Journal on Engineering Applications, 11(2), 73–80. doi:10.15866/irea.v11i2.22603.

[6] Mortezaei, A., & Ronagh, H. R. (2012). Plastic hinge length of FRP strengthened reinforced concrete columns subjected to both far-fault and near-fault ground motions. Scientia Iranica, 19(6), 1365-1378. doi:10.1016/j.scient.2012.10.010.

[7] Bayrak, B., Akarsu, O., Kaplan, G., & Aydin, A. C. (2023). The plastic hinge length prediction of RC members by using ANN. Sadhana - Academy Proceedings in Engineering Sciences, 48(3). doi:10.1007/s12046-023-02182-4.

[8] Opabola, E. A., & Elwood, K. J. (2023). Flexure-axial-shear interaction of ductile beams with single-crack plastic hinge behaviour. Earthquake Engineering and Structural Dynamics, 52(7), 2115–2134. doi:10.1002/eqe.3873.

[9] Junior, O. de A. S., & Ramam Carvalho de Oliveira, D. (2024). Numerical simulation and experimental analysis of plastic hinge length of reinforced concrete columns under monotonic flexure and constant axial load. Structural Concrete. Portico. doi:10.1002/suco.202300122.

[10] Sthapit, R., & Bandelt, M. (2023). Experimental Characterization of Plastic Hinge Behavior from Flexure and Axial Effects. International Interactive Symposium on Ultra-High-Performance Concrete, 3(1), 77. doi:10.21838/uhpc.16690.

[11] Pham, P. A. H., & Hung, C. C. (2023). Assessment of plastic hinge length in reinforced concrete columns. Structure and Infrastructure Engineering, 1–16. doi:10.1080/15732479.2023.2263432.

[12] Almeida, J., & Bandelt, M. (2023). Effects of Axial Load and Tensile Strength on Reinforced UHPC Plastic Hinge Length. International Interactive Symposium on Ultra-High Performance Concrete, 3(1), 31. doi:10.21838/uhpc.16658.

[13] Sahebjam, K. (1984). The Effects of Steel Fibers on the Plastic Rotation Capacity and Properties of Reinforced Concrete Continuous Beams. Master Thesis, South Dakota State University, Brookings, United States.

[14] Herbert, A., & Sawyer, J. R. (1964). Design of concrete frames for two failure stages. ACI Structural Journal, 405-437.

[15] Corley, W. G. (1966). Rotational Capacity of Reinforced Concrete Beams. Journal of the Structural Division, 92(5), 121–146. doi:10.1061/jsdeag.0001504.

[16] Mattock, A. H. (1967). Discussion of "Rotational Capacity of Reinforced Concrete Beams." Journal of the Structural Division, 93(2), 519–522. doi.org/10.1061/jsdeag.0001678.

[17] Park, R., & Paulay, T. (1975). Reinforced Concrete Structures. John Wiley & Sons, Hoboken, United States. doi:10.1002/9780470172834.

[18] Zahn, F. A. (1985). Design of Reinforced Concrete Bridge Columns for Strength and Ductility. Ph.D. Thesis. University of Canterbury, Christchurch, New Zealand.

[19] Priestley, M. J. N., & Park, R. (1987). Strength of Ductility of Concrete Bridge Columns Under Seismic Loading. ACI Structural Journal, 84(1), 61–76. doi:10.14359/2800.

[20] Sheikih, S. A., & Khoury, S. S. (1993). Confined concrete columns with Stubs. ACI Structural Journal, 90(4), 414–431. doi:10.14359/3960.

[21] Lu, Y., Gu, X., & Guan, J. (2005). Probabilistic Drift Limits and Performance Evaluation of Reinforced Concrete Columns. Journal of Structural Engineering, 131(6), 966–978. doi:10.1061/(asce)0733-9445(2005)131:6(966).

[22] Moehle, J. (2015). Seismic Design of Reinforced Concrete Buildings. McGraw Hill, New York, United States.

[23] Paulay, T., and Priestley, M. J. N. (1992). Seismic Design of Reinforced Concrete and Masonry Buildings. John Wiley & Sons, Hoboken, United States. doi:10.1002/9780470172841

[24] Panagiotakos, T. B., & Fardis, M. N. (2001). Deformations of reinforced concrete members at yielding and ultimate. ACI Structural Journal, 98(2), 135–148. doi:10.14359/10181.

[25] Berry, M. P., Lehman, D. E., & Lowes, L. N. (2008). Lumped-plasticity models for performance simulation of bridge columns. ACI Structural Journal, 105(3), 270–279. doi:10.14359/19786.

[26] Gu, D. S., Wu, Y. F., Wu, G., & Wu, Z. S. (2012). Plastic hinge analysis of FRP confined circular concrete columns. Construction and Building Materials, 27(1), 223–233. doi:10.1016/j.conbuildmat.2011.07.056.

[27] Youssf, O., ElGawady, M. A., & Mills, J. E. (2015). Displacement and plastic hinge length of FRP-confined circular reinforced concrete columns. Engineering Structures, 101, 465–476. doi:10.1016/j.engstruct.2015.07.026.

[28] Pudjisuryadi, P., Tavio, & Suprobo, P. (2016). Axial compressive behavior of square concrete columns externally collared by light structural steel angle sections. International Journal of Applied Engineering Research, 11(7), 4655–4666.

[29] ACI 374.1-05. (2014), Acceptance Criteria for Moment Frames Based on Structural Testing and Commentary, American Concrete Institute, Michigan, United States.

[30] Ou, Y.-C., Tsai, M.-S., Liu, K.-Y., & Chang, K.-C. (2012). Compressive Behavior of Steel-Fiber-Reinforced Concrete with a High Reinforcing Index. Journal of Materials in Civil Engineering, 24(2), 207–215. doi:10.1061/(asce)mt.1943-5533.0000372.

[31] Gkournelos, P. D., Triantafillou, T. C., & Bournas, D. A. (2021). Seismic upgrading of existing reinforced concrete buildings: A state-of-the-art review. Engineering Structures, 240, 112273. doi:10.1016/j.engstruct.2021.112273.

[32] Sakai, K., & Sheikh, S. A. (1989). What do we know about confinement in reinforced concrete columns? (A critical review of previous work and code provisions). ACI Structural Journal, 86(2), 192–207. doi:10.14359/2705.

[33] Tavio, Machmoed, S. P., & Raka, I. G. P. (2022). Behavior of Square RC Columns Confined with Interlocking Square Spiral Under Axial Compressive Loading. International Journal on Engineering Applications, 10(5), 322–335. doi:10.15866/irea.v10i5.20655.

[34] Agustiar, Tavio, Raka, I. G. P., & Anggraini, R. (2018). Behavior of concrete columns reinforced and confined by high-strength steel bars. International Journal of Civil Engineering and Technology, 9(7), 1249–1257.

[35] Sabariman, B., Soehardjono, A., Wisnumurti, W., Wibowo, A., & Tavio, T. (2018). Stress-strain behavior of steel fiber-reinforced concrete cylinders spirally confined with steel bars. Advances in Civil Engineering, 2018, 1–8. doi:10.1155/2018/6940532.

[36] Soehardjono, A., Sabariman, B., Wisnumurti, & Wibowo, A. (2022). Contribution of Steel Fibers on Ductility of Confined Concrete Columns. International Journal of GEOMATE, 23(97), 188–195. doi:10.21660/2022.97.3483.

[37] FEMA 356. (2000). Prestandard and Commentary for the Seismic Rehabilitation of Buildings. Federal Emergency Management Agency, Washington, United States.

[38] Wu, Y. F., & Jiang, C. (2014). Effect of confinement on plastic hinge length of RC square columns. 23rd Australasian Conf. on the Mechanics of Structures and Materials, 9-12 December, 2014, Southern Cross University, Byron Bay, Australia.

[39] Sabariman, B., & Sofianto, M. F. (2017). Study of crack patterns in beam column joint due to upwards anchoring beam effect. AIP Conference Proceedings, 1855(040004), 1–8. doi:10.1063/1.4985500.

[40] ASCE/SEI 41-06. (2007). Seismic Rehabilitation of Existing Buildings. American Society of Civil Engineers, Reston, United States.

[41] SNI 2052:2017. (2017). Concrete Reinforcing Steel. Standard Nasional Indonesia, Jakarta, Indonesia. (in Indonesian).

[42] Scott, B. D., Park, R., & Priestley, M. J. N. (1982). Stress-Strain Behavior of Concrete Confined By Overlapping Hoops At Low and High Strain Rates. Journal of the American Concrete Institute, 79(1), 13–27. doi:10.14359/10875.

[43] Sabariman, B., Soehardjono, A., Wisnumurti, Wibowo, A., & Tavio. (2020). Stress-strain model for confined fiber-reinforced concrete under axial compression. Archives of Civil Engineering, 66(2), 119–133. doi:10.24425/ace.2020.131800.

[44] Kusuma, B., and Tavio. (2008). Unified Stress-Strain Model for Confined Columns of Any Concrete and Steel Strengths. International Conference on Earthquake Engineering and Disaster Mitigation, 2008.

[45] Machmoed, S. P., Tavio, & Raka, I. G. P. (2021). Performance of Square Reinforced Concrete Columns Confined With Innovative Confining System Under Axial Compression. International Journal of GEOMATE, 21(85), 137–144. doi:10.21660/2021.85.j2085.

[46] MacHmoed, S. P., Tavio, T., & Raka, I. G. P. (2020). Potential of new innovative confinement for square reinforced concrete columns. Journal of Physics: Conference Series, 1469(1), 1–7. doi:10.1088/1742-6596/1469/1/012027.

[47] Wibowo, A., Wilson, J. L., Lam, N. T., & Gad, E. F. (2014). Drift capacity of lightly reinforced concrete columns. Australian Journal of Structural Engineering, 15(2), 131-150. doi:10.7158/s13-002.2014.15.2

[48] Harris, H., & Sabnis, G. (1999). Structural Modeling and Experimental Techniques, Second Edition. CRC Press, Boca Raton, United States. doi:10.1201/9781420049589.

[49] Bae, S., & Bayrak, O. (2008). Plastic hinge length of reinforced concrete columns. ACI Structural Journal, 105(3), 290. doi:10.14359/19788

[50] Ou, Y. C., Kurniawan, R. A., Kurniawan, D. P., & Nguyen, N. D. (2012). Plastic hinge length of circular reinforced concrete columns. Computers and Concrete, 10(6), 663–681. doi:10.12989/cac.2012.10.6.663.